Time-Resolved Measurement of Propagating Spin Waves in Ferromagnetic Thin Films

M. Covington,* T. M. Crawford, and G. J. Parker
Seagate Research, 1251 Waterfront Place, Pittsburgh, Pennsylvania 15222
(Received 27 February 2002; published 13 November 2002)

We measure the propagation of spatially localized spin waves in NiFe thin films through local inductive detection of the dynamic magnetization. A pulsed magnetic field excites a linear superposition of spin wave modes with a distribution that is predominantly driven by the spatial dependence of the in-plane excitation field. The results of numerical micromagnetic calculations exhibit excellent agreement with experiment and show that a comprehensive account of spatial nonuniformity and propagation is necessary to accurately measure the intrinsic damping rate.

DOI: 10.1103/PhysRevLett.89.237202 PACS numbers: 75.30.Ds, 75.50.Ss, 75.70.Ak, 76.50.+g

Spin waves are the fundamental dynamic magnetic excitations in ferromagnets [1–5]. Yet, after years of study, a comprehensive understanding of the time-domain response and the microscopic relaxation mechanisms of spin waves is unresolved. Recent advances in experimental time-domain techniques and computational capability are driving more accurate studies of magnetization dynamics in order to understand these basic physical issues. It is well known that abrupt magnetic field pulses will induce the localized electrons in a ferromagnet to coherently precess [6–8]. However, while new techniques have enabled direct observation of magnetization precession and captured spatial nonuniformity in the dynamic response, a quantitative description of the number and distribution of spin wave modes excited by an arbitrary pulsed field is still undetermined. Furthermore, comparisons of these experimental data to numerical calculations of the dynamic response via the Landau-Lifshitz-Gilbert (LLG) equation of motion typically neglect spatial nonuniformity. More sophisticated computations of the LLG equation are needed to infer the physical parameters of spin waves of arbitrary wavelength. The effects of interference and propagation can then be separated from the damping rate. An accurate determination of the phenomenological parameters in the LLG equation will then enable valid comparisons to microscopic theories of elementary dissipation mechanisms, such as spin wave scattering with phonons, electrons, and other spin waves [9].

Spin waves have been studied for many years by the nonlocal techniques of ferromagnetic resonance (FMR) and Brillouin light scattering (BLS) that measure relatively large volumes of material in the frequency domain [4,10,11]. While these techniques have measured the allowed manifold of spin wave excitations for a variety of material systems and geometries, propagation and relaxation can only be inferred through model dependent analysis. In contrast, new time-domain optical [6,8] and inductive techniques [7] allow the dynamic magnetization to be directly measured as it evolves in time, with a spatial resolution that far surpasses that of FMR and BLS. In this Letter, we extend the inductive technique by miniaturizing the transmission lines to enable us to excite and measure spatially localized propagating spin waves. We then compare the data to results of a numerical micromagnetic model and show that a systematic analysis is able to describe a wide range of behavior with the same set of material parameters.

We excite spin waves with pulsed magnetic fields from current carrying wires and measure the dynamic magnetization by inductive detection [7]. Figure 1(a) shows a device consisting of two nominally 50 Ω asymmetric coplanar strip (ACPS) transmission lines that overlay two patterned 475 μm squares of NiFe that have thicknesses of either 27 or 104 nm. The magnetic films are deposited onto a planarized surface, patterned into squares, and then have a 0.54 μm thick insulator deposited on top to isolate the squares from the waveguides. We make connections to the device via wide bandwidth coax-to-ACPS probes and touch down where the conductors expand into large pads. Voltage pulses with rise time

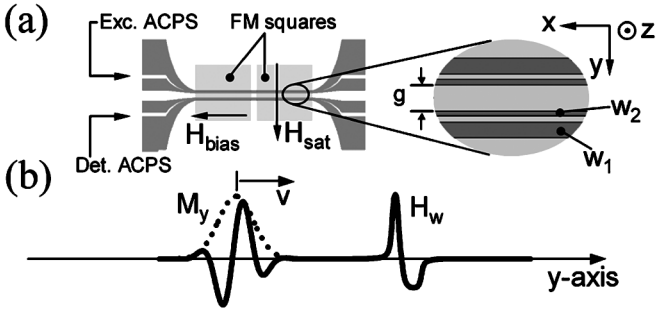

FIG. 1. Schematic of the experimental geometry. (a) Two ACPS transmission lines overlay ferromagnetic squares having uniaxial anisotropy in the x direction. The conductor dimensions in the narrow region are $w_2 = 3$ μm and $w_1 = 9$ μm, and they are separated by 2 μm. The gap, g, ranges from 2.5 to 50 μm. The fields H_{bias} and H_{sat} are produced by a set of Helmholtz coils. (b) Schematic of the magnetostatic wave packet, M_y, and the in-plane field, H_w, from the equal and opposite currents flowing through the ACPS. The dotted line is the Gaussian amplitude and the solid line is the full shape of M_y.

 0031-9007/02/89(23)/237202(4)$20.00

<100 ps are launched onto the ACPS centered down the middle of the squares, referred to as the excitation waveguide, while the inductive voltage can be measured from either this ACPS or the other ACPS, referred to as the detector waveguide, spaced laterally a distance g from the excitation waveguide. We study propagating waves by measuring a set of devices in which g varies from 2.5 to 50 μm from device to device.

All measurements are done in the time domain by detecting the inductive voltage with an 18 GHz bandwidth sampling oscilloscope. The waveforms are measured with a two-step process. We first measure the voltage with a 150 Oe saturation field along the pulsed field (or y) direction that pins the magnetization. We then subtract this reference waveform from those taken with a bias field applied along the x direction to acquire waveforms that are related to the components of the dynamic magnetization orthogonal to the ACPS [7]. Finally, in order to improve signal to noise, we take the average of 1024 waveforms to produce one waveform.

With the bias field on, the field pulse produces a sinusoidal inductive voltage in the excitation ACPS that decays to zero in the same qualitative manner that has been reported elsewhere [6,7]. This is shown in Fig. 2. In contrast, the inductive voltage from the detector ACPS, where the ferromagnet is *not* being driven by the pulsed field, responds quite differently. The waveforms exhibit a delay before the magnetization begins to precess that increases with increasing waveguide separation [12]. Furthermore, the rise time to maximum amplitude increases with increasing separation. These data are acquired with impulse excitation, but the response from the detector ACPS is equivalent with step pulse excitation. Although not shown, the inductive response is field dependent, and we observe an increase in the precessional frequency, delay, and rise time with increasing bias field. Lastly, we observe similar data from devices with 27 nm NiFe, albeit with different precessional frequencies and delay times.

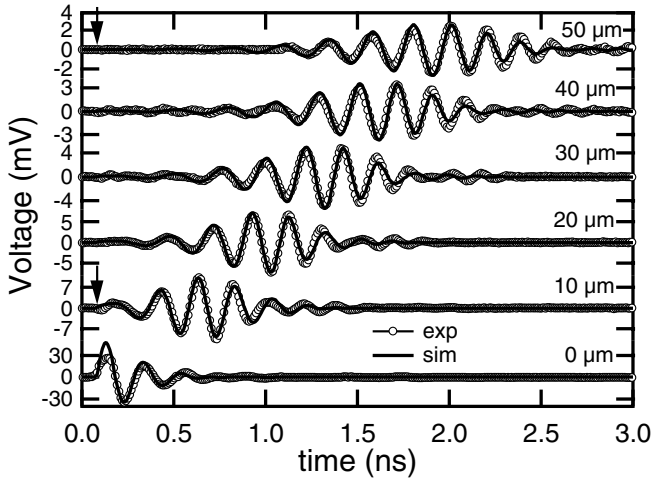

FIG. 2. Inductive voltage as a function of distance g from the excitation waveguide for devices with 100 nm NiFe at a 100 Oe bias field. The label "0 μm" indicates the response from the excitation ACPS. The arrows show when the excitation ACPS is pulsed for all devices.

We performed numerical micromagnetic calculations using Landau-Lifshitz theory in order to gain insight into the data. The computation models the magnetization dynamics as

$$d\mathbf{m}/dt = -\frac{\gamma}{1+\alpha^2}\mathbf{m} \times [\mathbf{H}_{\text{eff}} + \alpha\mathbf{m} \times \mathbf{H}_{\text{eff}}], \quad (1)$$

where $\mathbf{m} = \mathbf{M}/M_s$ is the unit magnetization vector, M_s is the (constant) saturation magnetization, γ is the gyromagnetic ratio, and α is the phenomenological Gilbert damping coefficient. All relevant terms are included in the effective field given by

$$\mathbf{H}_{\text{eff}} = \mathbf{H}_{\text{d}} + \frac{2A}{M_s}\nabla^2\mathbf{m} + \frac{2K}{M_s}(\mathbf{m}\cdot\mathbf{c})\mathbf{c} + \mathbf{H}_{\text{b}} + \mathbf{H}_{\text{p}}, \quad (2)$$

where the first term is the magnetostatic field ($\mathbf{H}_{\text{d}} = -\nabla\Phi$, $\nabla^2\Phi = 4\pi M_s \nabla\cdot\mathbf{m}$), A is the exchange constant, K is the uniaxial anisotropy constant, and $\mathbf{c}$ is the uniaxial direction. The remaining terms are the uniform bias and nonuniform pulse fields, respectively. In these simulations, the magnetization is uniformly discretized through the thickness and width (z and y) while the length has assumed translational symmetry. Therefore, efficient fast Fourier transforms can be used to calculate the volume averaged $\mathbf{H}_{\text{d}}$ in each computational cell of unit length and the exchange field is found from a simple 5-point Laplacian stencil. The volume averaged pulse field, $\mathbf{H}_{\text{p}}$, is found analytically from Biot-Savart assuming a spatially uniform current in the thin excitation ACPS with the temporal behavior determined by experimental observation. Equation (1) is integrated semi-implicitly with a fixed time step of 0.1 ps. The inductive voltage is calculated via reciprocity, where the flux is proportional to the overlap integral of the magnetization with the field from a fictitious current in the wires of the ACPS [7]. Since the experimental inductive coupling efficiency is unknown, the simulations are scaled by an overall constant factor to match the experimental amplitude.

The numerical data, also shown in Fig. 2, capture all of the salient features of the data. The computation uses $A = 1.6 \times 10^{-6}$ erg/cm. The saturation magnetization $4\pi M_s = 10$ kG and the anisotropy field $H_{\text{k}} \equiv 2K/M_s = 4$ Oe are determined from independent measurements of sheet films. The value of $\gamma = 19.91 \times 10^6$ rad/s/Oe (Landé g factor of 2.26) is extracted from the slope of the f_p^2 versus H_{b} curve acquired from conventional time-domain measurements of spin precession in the same material (f_p is the precessional frequency) [7]. A simulated bias field of $H_{\text{b}} = 105$ Oe produces the best agreement with the data taken in a 100 Oe field, although this discrepancy can be easily accounted for by the 10%

uncertainty of the measured value of M_s. The decay of the waveform amplitude with distance yields a damping coefficient of $\alpha = 0.0097$, which is consistent with the range of values previously measured in NiFe [4,6,7]. Lastly, the approximation of infinite length along the wire is supported by observations that the experimental frequencies and waveforms from ensembles of 100 μm squares are very similar to those measured from 475 μm squares, so the boundaries of the squares have negligible impact on the underlying physics [13].

The data in Fig. 2 show that these spatially localized wave packets are damped and spread in time. Additional data confirm the linear behavior of the spin waves. First, we have launched two pulses with variable delay and amplitude onto the excitation and detector waveguides and have shown that the two wave packets obey linear superposition [14,15]. Second, the amplitude of the inductive voltage scales linearly with pulsed field amplitude and the frequency and decay rate are independent of a pulsed field up to $H_p \sim H_b$. So, the response remains linear even for relatively large H_p. This applies to both step and impulse fields and is independent of whether the excitation or detector waveguide measures the voltage. Third, the simulated waveforms exhibit this same scaling with H_p.

So, despite the inherent nonlinearity of ferromagnetism, our experiment constitutes a linear system. We use this fact to fit our data with an analytical model that describes the wave packet as a linear superposition of spin waves. We approximate the wave packet with one magnetization component, M_y, having a sinusoidally modulated Gaussian amplitude, which is supported by the micromagnetic simulation. The wave packet propagates along the y direction and consists of a Gaussian distribution of wave vectors that is $2/\delta$ in width and centered about k_0. The corresponding spatial amplitude is also Gaussian and the full wave packet is given by

$$M_y = \frac{C\exp(-t/\tau)}{\delta^4 + \beta^2 t^2}\exp\left[\frac{-\delta^2(y-\nu t)^2}{4(\delta^4+\beta^2 t^2)}\right] \times \cos(k_0 y - \omega t + \phi). \quad (3)$$

The parameter C is a constant while $\nu = \partial\omega/\partial k|_{k_0}$ and $\beta = \frac{1}{2}\partial^2\omega/\partial k^2|_{k_0}$ are the coefficients of the first and second order terms, respectively, in the Taylor expansion of the nonlinear dispersion relation, $\omega(k)$. We also include a phenomenological exponential decay over a characteristic time τ to account for intrinsic damping effects. As with the micromagnetic simulation, the inductive voltage is calculated via reciprocity, and a schematic of the model is shown in Fig. 1(b).

The micromagnetic calculations imply that only magnetostatic fields are relevant since the results are the same regardless of whether or not the exchange interaction is included. The dispersion relation for magnetostatic waves propagating orthogonally to the magnetization is given by

$$\omega = \gamma\{4\pi M_s(H_k + H_b) + (2\pi M_s)^2[1 - \exp(-2kd)]\}^{1/2}, \quad (4)$$

where d is the thickness of the film and the other parameters have been previously defined [10,11,16]. We use Eqs. (3) and (4) to simultaneously fit the five waveforms from the detector ACPS ($10\ \mu\text{m} \le g \le 50\ \mu\text{m}$) acquired at the same bias field with the same set of parameters: amplitude (proportional to C), δ, k_0, and ϕ. The decay time τ is fixed and is determined from the same conventional time-domain inductive measurements used to determine γ.

The results of the analytical model complement our numerical results, and the data are shown in Fig. 3. The field dependence of the wave vector k_0 is consistent with the bias field dependence of the precessional frequency, in which the slope of the f_p^2 versus H_b curve is greater than $\gamma^2 M_s/\pi$. Another point is the relation between the population of spin wave modes and the wave vectors comprising the spatially dependent in-plane excitation field. The data in Fig. 3 indicate that the wave packet is centered about $k_0 \sim 0.25$–$0.30\ \mu\text{m}^{-1}$ with a distribution of modes over $2/\delta \sim 0.35\ \mu\text{m}^{-1}$. In comparison, the Fourier transform of the in-plane excitation field consists of a distribution of wave vectors centered around $\sim 0.29\ \mu\text{m}^{-1}$ with a full width at half maximum of $\sim 0.44\ \mu\text{m}^{-1}$. Hence, the spatially inhomogeneous pulse field is the predominant driver in creating the spatial nonuniformity of these linear spin waves [17,18].

The spatial nonuniformity, propagation, and potential decoherence arising from a distribution of $k > 0$ modes are commonly neglected in the analysis of time-domain data [6–8]. However, our data show the potential errors

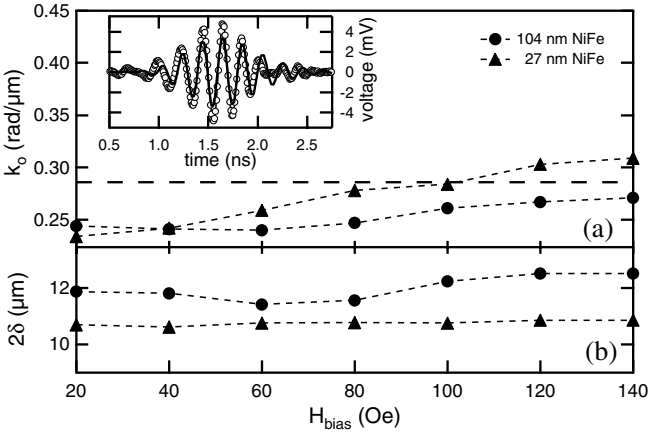

FIG. 3. Bias field dependence of the global fit parameters. (a) Wave vector. The dashed line indicates the peak location in the Fourier transform of the in-plane excitation field. (b) The initial $1/e$ point of the Gaussian wave packets. The inset shows an example of the agreement between experiment (open circles) and the fit (solid line) for the 100 nm NiFe device at 100 Oe with $g = 30\ \mu$m.

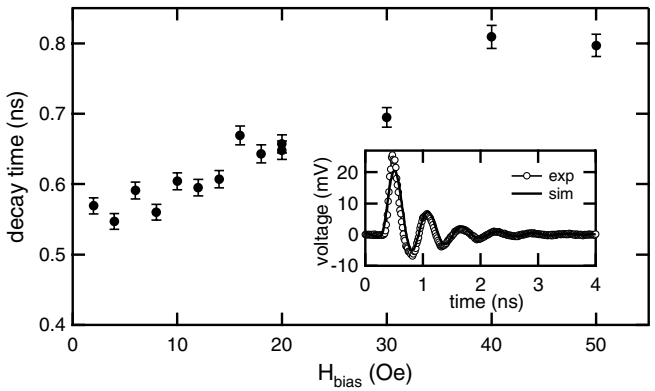

FIG. 4. Exponential decay time versus bias field for a device with a large CPW overlaying a 1 mm square of 100 nm thick NiFe, as described in the text. The inset shows experimental data (open circles) and the micromagnetic simulation (solid line) for a 16 Oe bias field.

involved with the assumption of a single, static mode. The data from the excitation ACPS (labeled "0 μm" in Fig. 2) provide a dramatic example because the voltage decays about 3 times faster than that implied by the damping rate (proportional to α). We also observe these effects in large devices on the same wafer. Figure 4 shows the fitted exponential decay time from a 1 mm square of NiFe driven by a coplanar waveguide (CPW) having a 100 μm center conductor and a 600 μm width between the outer edges of the ground planes. This decay time, extracted from the voltage peaks in the absolute value of the waveforms, would be inversely proportional to α if we excited small angle precession of the stationary, uniform mode [7] and thus would imply a field dependent α. Additional effects, such as nonlinearity [5,7], are usually invoked in order to describe this type of behavior. In contrast, we model this device micromagnetically using the same material parameters as those used to model the localized spin waves. The computation avoids simplifying assumptions and can fully account for the field dependent decay time using the same field independent α of 0.0097 used to describe the localized wave packets. These data indicate that the decrease in the decay time occurs because finite k spin waves propagate away from the detection region of the CPW, which is field dependent given the nonlinear dispersion relation of Eq. (4). This is supported by experimental observations of similar effects at the edge of a device of comparable size [19]. Hence, the decay time is not necessarily inversely proportional to α.

In conclusion, we observe linear propagating magnetostatic waves in a dispersive ferromagnetic medium. The spatial nonuniformity of the wave packets is predominantly driven by the spatial profile of the in-plane pulse field. We demonstrate that a single set of physical parameters, including α, can consistently describe magnetostatic waves spanning an order of magnitude in wavelength. From our combined data, we assert that a comprehensive understanding of the spatial and temporal aspects of spin waves is required before a physically meaningful measurement of the damping rate can be made.

We wish to acknowledge very useful discussions with A. Rebei, R. D. McMichael, and T. J. Silva.

*Electronic address: Mark.Covington@seagate.com

[1] C. Herring and C. Kittel, Phys. Rev. **81**, 869 (1951).
[2] C. Kittel, Phys. Rev. **110**, 1295 (1958).
[3] R. W. Damon and J. R. Eshbach, J. Phys. Chem. Solids **19**, 308 (1961).
[4] C. E. Patton, Phys. Rep. **103**, 251 (1984).
[5] A. H. Morrish, *The Physical Principles of Magnetism* (IEEE, New York, 2000).
[6] W. K. Hiebert, A. Stankiewicz, and M. R. Freeman, Phys. Rev. Lett. **79**, 1134 (1997).
[7] T. J. Silva *et al.*, J. Appl. Phys. **85**, 7849 (1999).
[8] Y. Acremann *et al.*, Science **290**, 492 (2000).
[9] H. Suhl, IEEE Trans. Magn. **34**, 1834 (1998).
[10] C. Mathieu *et al.*, Phys. Rev. Lett. **81**, 3968 (1998).
[11] J. Jorzick *et al.*, Phys. Rev. B **60**, 15 194 (1999).
[12] Capacitive coupling between probe pins leads to an induced voltage in the detector ACPS whenever the excitation ACPS is pulsed. This voltage is the same from device to device, and it induces a reproducible small amplitude spin precession (~ 0.6 ns in duration) that we subtract from all waveforms.
[13] When detecting at the edge ($g = 40$ μm) the waveform is qualitatively consistent with reflection from a boundary with at least some pinning of M_y.
[14] T. M. Crawford, P. Kabos, and T. J. Silva, Appl. Phys. Lett. **76**, 2113 (2000).
[15] M. Bauer *et al.*, Appl. Phys. Lett. **76**, 2758 (2000).
[16] A. Rebei and G. J. Parker (unpublished).
[17] R. L. White and I. H. Solt, Phys. Rev. **104**, 56 (1956).
[18] T. M. Crawford, M. Covington, and G. J. Parker, Phys. Rev. B (to be published).
[19] T. J. Silva, M. R. Pufall, and P. Kabos, J. Appl. Phys. **91**, 1066 (2002).